HHS Public Access

Author manuscript

Mol Cancer Res. Author manuscript; available in PMC 2018 January 01.

Published in final edited form as:

Mol Cancer Res. 2017 January ; 15(1): 93–105. doi:10.1158/1541-7786.MCR-16-0163.

Exosomal Annexin A2 Promotes Angiogenesis and Breast Cancer Metastasis

Sayantan Maji[1,3,*], **Pankaj Chaudhary**[1,3], **Irina Akopova**[2], **Phung M Nguyen**[2], **Richard J Hare**[5], **Ignacy Gryczynski**[2], and **Jamboor K. Vishwanatha**[1,3,4]

[1]Department of Molecular and Medical Genetics, University of North Texas Health Science Center, Fort Worth, Texas

[2]Department of Cell Biology and Immunology, University of North Texas Health Science Center, Fort Worth, Texas

[3]Institute for Cancer Research, University of North Texas Health Science Center, Fort Worth, Texas

[4]Texas Center for Health Disparities, University of North Texas Health Science Center, Fort Worth, Texas

[5]Plaza Medical Center of Fort Worth, Texas

Abstract

Tumor-derived exosomes are emerging mediators of tumorigenesis and tissue-specific metastasis. Proteomic profiling has identified Annexin A2 as one of the most highly expressed proteins in exosomes; however, studies focused on the biological role of exosomal-AnnexinA2 (exo-AnxA2) are still lacking. In this study, mechanistic insight was sought regarding exo-AnxA2 and its function in angiogenesis and breast cancer metastasis. Multiple in vitro and in vivo techniques were used to study the role of exo-AnxA2 in angiogenesis. Using atomic force microscopy (AFM) and Western blotting, exo-AnxA2 expression was characterized in normal and breast cancer cells. In addition, organ specific metastatic breast cancer cells and animal models were used to define the role exo-AnxA2 in breast cancer metastasis. Results revealed that exo-AnxA2 expression is significantly higher in malignant cells than normal and pre-metastatic breast cancer cells. In vitro and in vivo studies demonstrated that exo-AnxA2 promotes tPA-dependent angiogenesis. Furthermore, in vivo analysis indicated that metastatic exosomes create a favorable microenvironment for metastasis and exo-AnxA2 plays an important role in this process, since priming with AnxA2-depleted exosomes reduces brain (~4-fold) and lung (~2-fold) metastasis. Upon delineating the mechanism it was discovered that exo-AnxA2 causes macrophage-mediated

[*]Corresponding author: Sayantan Maji, Ph.D., Address: 3500 Camp Bowie Blvd, Fort Worth, TX 76107. Phone: 817-735-0422, Fax: 817-735-0695.
Current address: Mayo Clinic, 4500 San Pablo Rd, Jacksonville, Florida, 32224, sayantan.maji@live.unthsc.edu

Conflict of interest: The authors declare no conflict of interest.

Author contributions: SM and JKV conceived the manuscript and the experimental protocols. IG and SM conceived of the AFM experiments. IA and SM performed the AFM studies. PN and SM performed all the injections. SM performed all the rest of the studies, analyzed the data and wrote the manuscript. PC helped with the experiments. RH analyzed the immunohistochemical staining of the tissues. JKV acquired funding and gave substantial contribution to conception and study design and in data interpretation as well as critically revised the manuscript for important intellectual content. All authors read and approved the final manuscript.

activation of the p38MAPK, NF-κB, and STAT3 pathways and increased secretion of IL-6 and TNF-alpha. These data demonstrate an important role for exo-AnxA2 in breast cancer pathogenesis.

Keywords

Exosomes; annexin A2; angiogenesis; breast cancer; metastasis

Introduction

Exosomes are membrane vesicles, 40–100 nm in diameter, secreted from almost all cell types under both physiological and pathological conditions. Tumor-derived exosomes possess immunosuppressive properties and can facilitate tumor growth, metastasis and the development of drug resistance; effects which can contribute to cancer pathogenesis. By stimulating angiogenesis (1), modulating stromal cells, and remodeling extracellular matrix (ECM) (2), (3), tumor-derived exosomes contribute to the establishment of a pre-metastatic niche and generate suitable microenvironments in distant metastatic sites (4). Furthermore, recent discoveries have shown that exosomes from gynecologic neoplasias, including ovarian cancer and breast cancer, contain metalloproteinases that have proteolytic activity, which aids in metastasis; thus exosomes were found to increase the rate of ECM degradation and augment tumor invasion into the stroma (5).

Annexin A2 (AnxA2) is a Ca^{2+}-dependent phospholipid-binding protein associated with the plasma membrane and the endosomal system. AnxA2 is up-regulated in breast cancer and implicated in many cancer-associated functions, including plasminogen activation, actin-cytoskeletal rearrangement (6), cellular migration, adhesion, and proliferation (7). Specifically, increased cell surface expression of AnxA2 has been shown to contribute to increased angiogenesis and ECM degradation (7), (8). AnxA2 acts as a co-receptor for tissue plasminogen activator (t-PA) and plasminogen, which can form heterotetrameric complexes on the surfaces of cells with the AnxA2 light chain – S100A10 or p11, and this stimulates generation of t-PA-dependent plasmin. Plasmin is a highly reactive enzyme that is physiologically involved in fibrinolysis and plays an important role in neoangiogenesis (8), (9, 10). Previously, it has been shown that AnxA2 is associated with the lipid rafts and influenced by intracellular Ca^{2+} levels and N-terminal phosphorylation at tyrosine-23 (11). We have previously shown that binding of AnxA2 to the lipid rafts is followed by its transport along the endocytic pathway to be associated with the intraluminal vesicles of the multivesicular endosomes. AnxA2-containing multivesicular endosomes then fuse directly with the plasma membrane, resulting in the release of the intraluminal vesicles into the extracellular environment, facilitating the exogenous transfer of AnxA2 from one cell to another; a novel pathway of extracellular transport of AnxA2 (11).

Proteomic profiling data from Exocarta (12) have indicated that AnxA2 is abundant in the exosomes. In addition, secreted AnxA2 levels has been shown to positively correlate with the invasiveness of breast cancer cells (13), however, to the best of our knowledge no study has explored the biological role of exosomal AnxA2 (exo-AnxA2), especially in cancer. In

the present study, we characterized exo-AnxA2 in a breast cancer progression model. In addition, using AnxA2 competitive inhibitory peptide LCKLSL (14, 15) as well as shRNA mediated knockdown of AnxA2, we showed that exo-AnxA2 promotes angiogenesis and organ specific metastasis; two of the key hallmarks of cancer.

Materials and Methods

Cell line models

For the comparative analysis of exo-AnxA2, a MCF10A progression model (received as a gift from Dr. Judith Christman, UNMC, Omaha, NE, USA) was used: MCF10A (non-malignant), MCF10AT (pre-malignant), and MCF10CA1a (malignant). For the metastasis studies, MDA-MB-231 (ATCC, Manassas, VA, USA) and its organ-specific metastatic variants (received as a gift from Dr. Joan Massagué, MSKCC (New York City, NY, USA) and shipped by the Antibody and Bioresource Core facility) were used: MDA-MB-831 (brain metastasis), and MDA-MB-4175 (lung metastasis). The cell lines were authenticated by performing STR analysis with the Promega PowerPlex® Fusion V1.0. All the cells tested negative for mycoplasma infection when tested with MycoAlert PLUS from Lonza (Basel, Switzerland). The cell lines were not re-authenticated by the authors.

Cell Culture

MCF10A cells were cultured as described in (14), MCF10AT and MCF10CA1a cells were cultured as described in (16), and MDA-MB-231, MDA-MB-831, and MDA-MB-4175 cells were cultured as described in (17). Pooled clonetics™ HUVEC-Umbilical Vein Endothelial Cells (Lonza, Basel, Switzerland) were grown in EGM™ Media plus bovine brain extract at 37°C in 5% CO_2.

Antibodies and reagents

The following antibodies were used: anti-AnxA2 (BD Biosciences, San Jose, CA, USA), anti-GAPDH, anti-CD81, anti-Arginase 1 (Santa Cruz Biotechnologies, Dallas, TX, USA), anti-phospho-p38 (Thr180/ Tyr182), anti-p38, anti-phospho-NFκB p65 (S536), anti-NFκB p65, anti-phospho-STAT-3 (Y705), anti-STAT-3, anti-MMP-9, anti-VEGF (Cell Signaling Technologies, Boston, MA, USA), anti-human vimentin (NCL-L-VIM-V9, Leica Biosystems, Wetzlar, Germany), anti-mouse CD31, anti-tPA, anti-VEGFR1 (Abcam, Cambridge, United Kingdom), anti-calnexin (Enzo, Farmingdale, NY, USA), anti-CD63 (Developmental Studies Hybridoma Bank, Univ. of Iowa, Iowa City, IA, USA), anti-uPA (R & D Biosystems, Minneapolis, MN, USA), anti-F4/80 (AbD Serotec, Raleigh, NC, USA), and 25-nm gold nanoparticle-tagged secondary anti-mouse antibody (Electron Microscopy Sciences, Hatfield, PA, USA). We also used protein A/G beads for immunoprecipitation (IP); (Santa Cruz Biotechnologies, Dallas, TX, USA), Versene (Gibco, Thermo Fisher Scientific, Waltham, MA, USA), India ink dye (American Master Tech, Lodi, CA, USA), Calcein-AM dye (Life Technologies, Thermo Fisher Scientific, Waltham, MA, USA), PKH26 (Sigma-Aldrich, St. Louis, MO, USA), Matrigel and matrigel-HC (BD Biosciences, San Jose, CA, USA), D-luciferin (Caliper Life Sciences, Waltham, MA, USA), LCKLSL and LGKLSL peptides (Bio Basic Inc. Markham, ON, Canada), and a mouse TNF-alpha and IL-6 ELISA kit (e-bioscience, San Diego, CA, USA).

Exosome isolation and characterization

Exosomes were isolated by ultracentrifugation (18) and labeled with PKH26 (Sigma Aldrich, St. Louis, MO, USA), as previously described (19). Secreted exosomes were quantified by measuring acetylcholinesterase activity (15). Electron microscopy (18) and atomic force microscopy (AFM) (20) of the exosomes were performed as previously published.

Migration, invasion, and angiogenesis assay

Migration and invasion assays were performed with BD Transwell invasion assay inserts, according to the manufacturer's protocol. The matrigel plug assay was performed as previously described (21). Briefly, 400 μl of matrigel (~20mg/ml) were injected subcutaneously, along with PBS, VEGF, or different exosome treatments with or without the peptides. After 12 days, the matrigel plugs were isolated and imaged. Half of the plugs were processed for immunohistological analysis and half were used for hemoglobin estimation by Drabkin's method, using a previously published protocol (22, 23). For all these assays we used LCKLSL inhibitory or LGKLSL control peptides as published previously (14, 15).

shRNA-mediated down-regulation of AnxA2

To downregulate exo-AnxA2, shRNA against AnxA2 (GIPZ Lentiviral Human ANXA2 and shRNA, GE Dharmacon, Lafayette, CO, USA) was used. Exosomes isolated from shAnxA2 and shControl cells were designated as AnxA2KD-Exo and Control-Exo, respectively.

Animal studies

The animals were procured under Institutional Animal Care and Use Committee (IACUC)-approved protocols and all the studies and experiments were carried out in accordance with the IACUC protocol for animal handling. 4- to 6-week-old female athymic nude mice (Harlan Laboratories, Indianapolis, Indiana, USA) were used for all the animal studies.

Priming of animals with exosomes

To study the role of exo-AnxA2 in metastasis, the animals were injected with PBS or exosomes from breast cancer cells stably transfected with sh-Control (Control-exo) or with sh-AnxA2 (AnxA2KD-exo). Priming was performed via regular injection of 100μg of exosomal proteins in 100μl PBS via the lateral tail vein, twice a week for four weeks.

Metastasis models

To check the role of exo-AnxA2 in promoting breast cancer metastasis, two different models were used: intravenous (lateral tail vein) lung metastasis and an intra-cardiac metastasis model. MDA-MB-231, MDA-MB-831, and MDA-MB-4175 cells were used for the metastasis study. At the end of exosome priming, the primed animals were challenged with the respective luciferase-positive breast cancer cells and the difference in the extent of organ-specific metastasis over time was studied via bioluminescence (BLI). At the end of the study, the animals were sacrificed and the organs were harvested and analyzed further by hematoxylin and eosin (H & E) staining and DAB immunostaining (anti-human vimentin) to stain the metastasized human breast cancer cells. Lung and brain sections were also

analyzed by a pathologist for the presence or absence of immunostaining in the organ stroma.

Intravenous (tail vein) injection (24, 25) and intracardiac inoculation (26) of luciferase-positive breast cancer cells were performed as previously published.

In vivo imaging of animals

In vivo animal imaging using an IVIS Lumina XR system (Caliper Life Sciences) was performed weekly, as previously published (26). In each study, identical exposure times were used to detect BLI among the different treatment groups.

Histological analyses of tissues: Hematoxylin and Eosin staining as well as immunohistological (IHC) analyses of paraffin blocked tissue sections were performed using standard procedures. Respective isotype matched mouse and rabbit normal IgG antibodies were used as controls for all immunostainings. Furthermore, for IHCs an additional Fc receptor-blocking step was performed to rule out the possibility that exosome treatment increases the expression of Fc gamma receptor, which might non-specifically bind primary antibodies used in the IHC.

ELISA for IL-6 and TNF-alpha

ELISA kits were purchased from eBioscience and ELISA was performed according to the manufacturer's protocol.

Immunoprecipitation and Signaling

For the IP experiment, 231-AnxA2KD cells were treated with PBS/231-AnxA2KD-exo or 231-Control-exo (100 μg protein) and returned to the incubator for 6 hrs. Next, the cells were washed with PBS and the membrane proteins were stripped via versene wash (0.5 mM EDTA and PBS buffer). The versene eluates were centrifuged at 10,000g for 15 min to remove any cell debris and immunoprecipitated with pro-cathepsin B antibody overnight and probed for AnxA2. For the signaling experiments, HUVEC endothelial cells were treated with PBS/231-AnxA2KD-exo or 231-Control-exo (100 μg protein) and returned to the incubator. After the incubation, the cells were washed, WCL was collected in NP40 lysis buffer, and Western blotting was performed with the designated antibodies. For tPA studies, HUVEC endothelial cells were pre-treated with PBS/tPA antibody (2μg/ml) or IgG control antibody (2μg/ml) for 2 hrs, followed by treatment with MDA-MB-231 exosomes (100μg) and kept for 6 hrs at 37°C. After incubation, the cells were fixed and photographed. The number of branch points/field and number of meshes/field were counted via NIH ImageJ software to quantify the angiogenic response.

Statistical Analysis

Results are expressed as arithmetic means ± SEM if not otherwise indicated. Values of $P \leq 0.05$ were considered statistically significant, as determined by the unpaired Mann–Whitney test, the two-tailed unpaired Student's *t*-test, or the Wilcoxon signed-rank test, where appropriate. (*) $p < 0.05$, (**) $p < 0.01$, (***) $p < 0.001$, and (****) $p < 0.0001$ for all the

figures. GraphPad Prism statistical software was used for all statistical analyses. NCSS Power analysis software was used for animal studies.

Results

Exo-AnxA2 correlates positively with the aggressiveness of breast cancer cells

To characterize exo-AnxA2 expression, we used the MCF10A breast cancer progression model, which consists of MCF10A (immortalized mammary epithelial cell line), MCF10AT (premalignant cell line generated by *HRAS* transformation of MCF10A), and MCF10CA1a (derived from poorly-differentiated malignant tumors of MCF10AT xenografts) cells (27). Western blotting of exosomal lysate from MCF10A, MCF10AT, and MCF10CA1a revealed that exo-AnxA2 levels highly correlated with the aggressiveness of the breast cancer cells, with lower levels in MCF10A, moderate levels in MCF10AT, and significantly higher levels in MCF10CA1a (Fig. 1A); however, the whole cell lysate (WCL) analysis of the progression model revealed no significant changes in the levels of AnxA2 in MCF10AT and MCF10CA1a (Supplementary Fig. S1H). Densitometry revealed that exo-AnxA2 levels were ~5-fold greater in MCF10CA1a exosomes than in MCF10A exosomes (Fig. 1B). Interestingly, the levels of other angiogenic markers, including Vascular Endothelial Growth Factor (VEGF), Urokinase-type Plasminogen Activator (uPA), and matrix metalloproteinase 9 (MMP9), were relatively unchanged (Supplementary Fig. 1G). CD81 was used as a specific exosomal marker and a loading control.

Expression of exo-AnxA2 is higher in MCF10CA1a exosomes than MCF10A exosomes

Scanning of exosomes in the MCF10A progression model by Atomic Force Microscope (AFM) revealed a higher surface expression of AnxA2 on the MCF10CA1a exosomes than the MCF10A exosomes, as depicted by increased surface binding of 25-nm gold nanoparticle-tagged anti-AnxA2 antibody (Fig. 1C). Quantification of the number of gold nanoparticles per field revealed almost ~5-fold greater binding of gold nanoparticles on MCF10CA1a exosomes than MCF10A exosomes (Fig. 1D). Surface topography analysis confirmed these findings, showing multiple peaks corresponding to higher gold nanoparticle binding in MCF10CA1a exosomes, but much less in MCF10A exosomes after treatment with AnxA2 antibody (Fig. 1E); indicating that MCF10CA1a exosomes have more AnxA2 surface expression than MCF10A exosomes. The exosomal marker CD63 and the endoplasmic reticulum (ER) marker calnexin served as positive and negative controls, respectively.

Exo-AnxA2 promotes angiogenesis

Since AnxA2 has been implicated in promoting angiogenesis previously (7, 14, 15), in the present study we investigated whether exo-AnxA2, once secreted from cells, is capable of promoting angiogenesis as well. In an *in vitro* model of angiogenesis, we compared the angiogenic potential of exo-AnxA2 in MCF10A, MCF10AT, and MCF10CA1a cells using LCKLSL and LGKLSL peptides (14, 15). The *in vitro* endothelial tube formation assay showed that exosome treatments resulted in ~4-fold, ~6-fold, and ~7.5-fold increases in the number of meshes per field and ~1.4-fold, ~1.8-fold, and ~2-fold increases in the number of branch points per field with MCF10A, MCF10AT, and MCF10CA1a exosomes, respectively

(Supplementary Figs. 2 and S2 A, C). Interestingly, exosome incubation with LCKLSL nullified the angiogenic effect of exo-AnxA2 (a ~3-fold decrease in the number of meshes per field and ~0.75-fold decrease in the number of branch points per field in the case of MCF10CA1a); however, treatment with LGKLSL had no effect (Supplementary Figs. 2, S2 A–D). Incubation of LCKLSL with MCF10A and MCF10AT exosomes showed similar effects (data not shown).

Endothelial cell migration and invasion is an important step in angiogenesis (28) and AnxA2-p11-tPA-mediated plasmin generation potently promotes this process (7). Thus, to further confirm the role of exo-AnxA2 in plasmin generation and angiogenesis, we studied the effect of exo-AnxA2 on the migration and invasion of HUVEC cells. HUVEC endothelial cells were added with the respective exosomes, with or without LCKLSL or LGKLSL, into the upper chamber of the transwell and incubated for 24 hrs. After incubation, the number of cells that migrated to or invaded the other side of the membrane was counted. Treatment with MCF10CA1a exosomes plus LCKLSL led to a significant decrease in both migration (~40%) and invasion (~30%) of HUVEC cells, compared to MCF10CA1a exosome treatment only or with LGKLSL (Fig. S1 J – L).

To confirm our *in vitro* findings and to study the pro-angiogenic role of exo-AnxA2 in a physiologically relevant setting, we performed an *in vivo* matrigel plug assay (21). Mice were injected subcutaneously with matrigel in the presence of PBS alone (negative control), matrigel mixed with VEGF (positive control), or matrigel mixed with respective exosome treatments. The LGKLSL or LCKLSL peptides were incorporated into the matrigel plugs in the presence of the exosomes. Twelve days after the implantation of matrigel, the mice were sacrificed and the matrigel plugs were isolated and imaged for angiogenesis. Half of the plugs were sectioned for immunohistological analysis to study blood vessel formation and CD31 (endothelial cell marker) staining. The remaining plugs were homogenized and their hemoglobin content was estimated to quantify angiogenesis.

Analysis of the matrigel plugs showed that MCF10CA1a exosome treatment induced significantly higher angiogenesis than the MCF10AT and MCF10A exosomes (Fig. 2 B). Hemoglobin estimation of the homogenized matrigel plugs confirmed these results, showing ~5-fold, ~14-fold, and ~ 24-fold increases in hemoglobin content when incubated with MCF10A, MCF10AT, and MCF10CA1a exosomes, respectively vs. PBS treatment (Fig. 2 C). Consistent with our *in vitro* findings, incubation of the matrigel plug-exosome mixture with LCKLSL resulted in a drastic decrease in angiogenesis, as evident from matrigel plug images (Fig. 2 B). Hemoglobin content analysis from MCF10CA1a exosome-treated homogenized matrigel plugs confirmed these results, showing a ~5-fold decrease with LCKLSL treatment, which did not occur with LGKLSL or exosome treatment alone (Fig. 2 D); injection of matrigel with MCF10A or MCF10AT exosomes plus LCKLSL had similar effects (Supplementary Fig. S2 E – F). H & E staining (Fig. S4 A – B) and DAB (3, 3'-diaminobenzidine) immunostaining (Fig. S4 C – D) of matrigel plug sections against endothelial marker CD31 (recruitment of CD31-positive endothelial cells indicates increased angiogenesis) confirmed our findings, showing less CD31-positive endothelial cells in all LCKLSL treatments than in all LGKLSL treatments (Fig. S4 A – D). Further, LCKLSL treatment markedly reduced the number of blood vessels in the plugs, compared to LGKLSL

treatment. We also reconfirmed our findings by knocking down AnxA2 levels in the exosomes in a different breast cancer cell line, MDA-MB-231. *In vitro* endothelial tube formation assays and *in vivo* matrigel plug assays were performed with exosomes after knocking down AnxA2 (231-AnxA2KD-Exo) and compared to control (231-Control-Exo). Quantification of the *in vitro* angiogenesis assay showed that 231-AnxA2KD-Exo treatment generated ~4.5-fold and ~3-fold decrease in the number of meshes per field and number of branch points per field, respectively, compared to 231-Control-Exo treatment (Supplementary Fig. S3 A – B). The matrigel plug assay with 231-AnxA2KD-Exo treatment also revealed ~5-fold less hemoglobin content on average per matrigel than 231-Control-Exo treatment (Supplementary Fig. S3 C – D).

Exo-AnxA2 promotes angiogenesis in a tPA dependent manner

To investigate the molecular mechanism by which exo-AnxA2 promotes angiogenesis, we performed a detailed analysis of the affected signaling pathways. We found that antibody-mediated blocking of tPA nullified the pro-angiogenic effects of exo-AnxA2. Incubation of tPA antibody-pretreated HUVEC endothelial cells with 231-Control-Exo showed a ~2.6-fold decrease in the number of meshes per field than did IgG control treatment (Fig. 3 A–B). Similarly, the number of branch points per field decreased ~2.75-fold after tPA antibody pretreatment, compared to IgG control (Fig. 3C). These results indicate that similar to cell surface AnxA2, exo-AnxA2 also mediates its pro-angiogenic effects via tPA, probably by acting as a receptor for both tPA and plasminogen (14, 15, 28).

Exo-AnxA2 promotes breast cancer metastasis to lungs

Although MCF10CA1a is a highly metastatic cell line, MDA-MB-231 and its organ-specific metastatic variants, MDA-MB-831 (brain metastatic) and MDA-MB-4175 (lung metastatic), are very well characterized for organ-specific metastatic studies (29–31). Thus, for our metastatic studies, we used MDA-MB-231, MDA-MB-831, and MDA-MB-4175 cells. We found that intravenous (tail vein) exosome injection led to organotropism of the breast cancer exosomes, since fluorescently-tagged MDA-MB-4175 lung metastatic exosomes showed ~5.5-fold more lung localization than MDA-MB-231 or MDA-MB-831 exosomes (Supplementary Fig. S5 B – C); this indicates possible mechanistic cross-talk between the exosomes and the homing organ, leading to organotropism.

For our organ specific metastatic studies, we knocked down AnxA2 by shRNA in MDA-MB-231, MDA-MB-831, and MDA-MB-4175 cells. Western blotting of the WCL (Fig.3 D) and the exosomal lysates (Fig. 3 E) showed the levels of AnxA2 in the specific fractions. Quantification is shown in Fig. 3F ; exosome designations for all the groups are given in Supplementary Fig. S3 E).

First, we tested the lung metastasis model by lateral tail vein injection. Challenge with 2×10^6 luciferase-positive MDA-MB-231-luc cells (tail vein) after one month of exosome priming showed increased lung metastasis in 231-Control-Exo-primed animals compared to 231-AnxA2KD-Exo-primed (~2-fold) or PBS-treated animals (~6-fold) (Fig. 3 G). Quantification of the number of metastatic lung nodules showed that priming with 231-Control-Exo resulted in ~12-fold and ~2.5-fold increases in the number of nodules,

compared to PBS-primed and 231-AnxA2KD-Exo-primed animals, respectively (Fig. 3 I , J). We confirmed our results with H & E staining and human vimentin immunostaining of the lung sections, which showed significant metastasis, having larger metastatic lung nodules in 231-Control-Exo-primed animals than 231-AnxA2KD-Exo-primed animals, which had much smaller metastatic nodules (Fig. 4 A–B).

We further studied the role of exo-AnxA2 in lung metastasis in a different metastatic model – intracardiac (ic) injection metastatic model. Challenge with 1×10^5 luciferase-positive MDA-MB-4175-luc cells after one month of exosome priming showed greater lung metastasis in 4175-Control-Exo-primed animals than in 4175-AnxA2KD-Exo-primed animals (~1.8-fold) or PBS-treated animals (~2.4-fold) (Fig. 3 H). Quantification of the number of metastatic lung nodules showed that priming with 4175-Control-Exo resulted in ~8-fold and ~2-fold more nodules than PBS- and 4175-AnxA2KD-Exo-primed animals, respectively (Fig. 3 K), similar to our MDA-MB-231-luc results, further confirming the important role of exo-AnxA2 in lung metastasis. These data clearly show that exo-AnxA2 promotes breast cancer metastasis to the lungs.

Exo-AnxA2 promotes breast cancer metastasis to brain

To study whether exo-AnxA2 promotes brain metastasis, we utilized two different experimental setups. First, we primed the animals with PBS, 831-AnxA2KD-Exo, or 831-Control-Exo and then challenged them with 1×10^5 MDA-MB-231-luc cells (ic). Bioluminescence imaging (BLI) of the animals revealed significant differences among the different treatment groups: animals primed with 831-Control-Exo showed increased brain metastasis when compared to 831-AnxA2KD-Exo-primed animals (~2-fold) or PBS-treated animals (~3.8-fold) (Fig. 4 C).

Next, we injected 1×10^5 MDA-MB-831-luc cells (ic) in PBS-, 831-AnxA2KD-Exo-, or 831-Control-Exo-primed animals. Similar to our MDA-MB-231-luc findings, we saw significant differences among the different treatment groups, but the differences were more pronounced than in the MDA-MB-231-luc-challenged animals. Animals primed with 831-Control-Exo showed significantly higher brain metastasis than 831-AnxA2KD-Exo-primed animals (~4-fold) or PBS-treated animals (~10-fold) (Fig. 4 D). We confirmed our results with H & E staining and human vimentin immunostaining of the brain sections, which showed significant macrometastasis in 831-Control-Exo-primed animals, whereas 831-AnxA2KD-Exo-primed animals showed micrometastasis (Fig. 4 E–F). In both of these brain metastatic studies, we found that exosome priming increased brain metastasis. Interestingly, in MDA-MB-231-luc-injected animals, PBS priming showed whole-body distribution of the cells, whereas 831-Exo priming led to greater localization of the cancer cells to the brain.

Furthermore, in both lung and brain metastatic models, we discovered that the respective exosome treatments led to a higher rate of organ-specific metastasis (photon flux vs. time) in Control-Exo-primed animals (high BLI, starting from 2 weeks) than their AnxA2KD-Exo counterparts, suggesting that exo-AnxA2 priming creates a microenvironment that leads to faster and higher brain and lung metastases (Fig. 5 A–B).

Exo-AnxA2 creates a pre-metastatic niche via activation of p38, NFκB, and STAT 3 pathways

Upon investigating the mechanism by which exo-AnxA2 promotes metastasis, we found that it co-localizes with pro-cathepsin B on the cell surface (Figure 5 C–E). Immunoprecipitation with cathepsin antibody in 231-AnxA2KD-Exo and 231-Control-Exo treated 231-AnxA2KD cells showed higher pull-down (~2.25 fold) of AnxA2 in the latter, indicating that increased exo-AnxA2 treatment can lead to an increased co-localization with pro-cathepsin B.

Previously, (Swisher et al.) have shown that secreted AnxA2 can activate macrophages for IL-1, IL-6, and TNF-α secretion through MAP kinase and NF-κB dependent pathways (32, 33). Based on this we wanted to investigate whether exo-AnxA2 can activate macrophages, leading to the activation of pro-inflammatory signaling cascades. F4/80 staining of the lung tissues showed that 231-Control-Exo-primed animals had significantly greater positive staining for the activated macrophage marker than 231-AnxA2KD-Exo-primed animals, indicating that exo-AnxA2 priming leads to the activation of macrophages (Fig. 5 F). Furthermore, ELISA quantification of the lungs 24 hrs after (tail vein) exosome injection showed that secretion of both IL-6 and TNF-alpha was higher in 231-Control-Exo-primed animals (~3.3-fold and ~4-fold, respectively) than in 231-AnxA2KD-Exo-primed animals (Fig. 5 G).

Our preliminary study in HUVEC cells revealed that 231-Control-Exo treatment activates NFκB, p38 and STAT3 signaling cascades (~2.5-fold, ~2.2-fold, and ~1.5-fold greater than control, respectively,) but 231-AnxA2KD-Exo treatment does not (Fig. S6 B – C). Western blotting of lung extracts from exosome-primed animals confirmed our finding; control-Exo-primed animals had ~2.1-, ~2.2-, and ~1.75-fold greater expression of phospho-NFκB, phospho-p38, and phospho-STAT3, respectively, than AnxA2KD-Exo-primed animals (Fig.S6 D – E). To study the signaling pattern, we performed DAB immunostaining of the brain and lung sections. Sections from the 231-Control-Exo-primed animals showed higher phospho-STAT3 and phospho-p38-NFκB immunostaining in the lung and brain stroma than 231-AnxA2KD-Exo-primed animals (Fig. 6 and 7); as reported earlier, MMP9 staining of the tissues also showed similar results. Analysis of the lung staining revealed that the expression of phospho-STAT3 and phospho-p38-NFκB were mostly confined to the alveolar network and interstitial air sacs, but were not in bronchial epithelial cells.

Discussion

Recent studies have delineated important roles of exosomal cargo in physiological processes as well as various disease pathogenesis. In the present study, we characterized exo-AnxA2 in breast cancer cell lines and explored its function in promoting angiogenesis and breast cancer metastasis independently. Characterization of exo-AnxA2 levels in breast cancer cells revealed that highly metastatic MCF10CA1a (Fig. 1 A) and MDA-MB-231 (Supplementary Fig. S1 I) cells have significantly higher expression than MCF10A and MCF10AT cells. This confirms a previous finding by Jeon et al. where they reported increased levels of AnxA2 in the media of invasive triple-negative human breast cancer cells, demonstrating a

positive correlation of secreted AnxA2 with the invasive phenotype of breast cancer cells (13).

AnxA2 along with p11 and tPA has been reported to be a potent inducer of angiogenesis (7, 8). tPA binds to amino acid residues at positions 7–12 in the N-terminus of AnxA2, corresponding to the site LCKLSL (14). Sequential mutations in the N-terminus of AnxA2 indicated that the cysteine residue at position 8 is crucial for the binding of tPA to AnxA2; mutation of this residue significantly reduces the efficiency of tPA binding to AnxA2. Previously, among an array of synthetic peptides containing cysteine residues and spanning the N-terminus of AnxA2, the hexapeptide LCKLSL, which is identical in sequence to the tPA-binding site of AnxA2, was >95% efficient in competitively inhibiting tPA binding to AnxA2; however, replacing the cysteine residue with a glycine residue nullifies any inhibitory effect (14). In the present study, using LGKLSL control peptide and LCKLSL inhibitory peptide to specifically inhibit the function of AnxA2 (14, 15) we investigated whether exo-AnxA2 can promote angiogenesis once secreted from the cells. Utilizing various *in vitro* and *in vivo* models we found that exo-AnxA2 is a potent inducer of angiogenesis and its effect can be blocked by LCKLSL inhibitory peptide. We also found that the pro-angiogenic effects of exo-AnxA2 can be attenuated by application of tPA antibody indicating that tPA is an important mediator of exo-AnxA2 mediated angiogenesis.

Independently, we investigated the role of exo-AnxA2 in promoting organ specific breast cancer metastasis. Evidence suggests that systemic factors (exosomes, microvesicles, etc.) from the primary tumor are involved in pre-metastatic niche formation, a specialized microenvironment that forms at the sites of future metastases and promotes the survival and outgrowth of disseminated tumor cells (34). Using an animal model, Peinado et al. showed, for the first time, that melanoma exosomes educate bone marrow progenitor cells toward a pro-metastatic phenotype through MET (35). Based on this, we used a model, which, for the first time, showed that priming (regular tail vein injections of exosomes) of the animals with breast cancer exosomes can promote organ-specific breast cancer metastasis and that exo-AnxA2 plays a major role in this process (36). Collectively, our lung and brain metastasis data suggest that qualitative differences in exosome content can affect metastatic potential and organotropism. In addition we found that exo-AnxA2 priming leads to a faster rate of organ specific metastasis (Fig. 5 A–B); however, quantification of the number of exosomes in the lungs (231 and 4175) and brain (831) showed no significant differences between 231-AnxA2KD-Exo-primed and 231-Control-Exo-primed animals (Supplementary Fig. 6 F – H) indicating that the differences in exo-AnxA2 levels were primarily responsible for the difference in the extent of metastasis. Furthermore, increased brain-specific metastasis also indicates that exosomes can cross the blood brain barrier, as reported previously (37), and form a pre-metastatic niche.

Investigating the mechanism by which exo-AnxA2 may promote breast cancer metastasis, we found that exo-AnxA2 forms a pre-metastatic niche by activating STAT3 and p38-NFκB. Swisher et al. previously showed that treatment of macrophages by AnxA2- tetramer leads to a MAP-kinase dependent activation of inflammatory cytokine (IL-6, TNF-alpha and IL-10) transcription by 3 hrs. Interestingly, in our study, ELISA analysis of lungs tissue revealed that tail vein injection of exo-AnxA2 leads to activation of IL-6 and TNF-alpha 24

hrs after injection. We believe these secreted cytokines from macrophages promote tumor progression and metastasis, as reported in pancreatic cancer (38) and hepatoma (39). Similar results were obtained with 831-Control-Exo- and 4175-Control-Exo-primed animals (data not shown).

In addition, priming with 231-Control-Exo also showed increased levels of VEGFR1 in both lung and brain sections, compared to PBS-primed animals (Supplementary Fig. S5 D), indicating that cancer exosomes can up-regulate VEGFR1 expression, which has been previously linked with breast cancer metastasis (40, 41).

We also discovered that exo-AnxA2 priming leads to increased MMP9 expression in the tissues (Fig. 6 and 7); possibly further contributing to extracellular proteolysis and angiogenesis.

There is also a possibility that in addition to creating a pre-metastatic niche, exo-AnxA2 secreted by cancer cells can participate in autocrine and paracrine signaling, acting on the cancer cells themselves and promoting migration, invasion, and metastasis. A preliminary analysis of the effect of exo-AnxA2 on 231-AnxA2KD breast cancer cells shows that, once taken up, exo-AnxA2 co-localizes with pro-cathepsin B on the cell surface (Fig. 5 C–E). Western blotting of the IP lysates showed much greater AnxA2 pull-down in 231-Control-Exo-treated cells than 231-AnxA2KD-Exo-treated cells. Previously we have shown that exo-AnxA2 is internalized and can be recycled to be expressed on the cell surface (15); we believe that internalized exo-AnxA2 probably exists in a complex with pro-cathepsinB, tPA, plasminogen, and p11, as reported earlier (42), and helps in ECM degradation, plasmin generation, and metastatic dissemination of the breast cancer cells. However, further studies are needed to delineate the detailed mechanism by which exo-AnxA2 promotes breast cancer metastasis.

Although we were able to achieve significant knockdown of AnxA2 in our cells and exosomes, we were not able to completely remove AnxA2 from our treatments. Thus one of the major drawbacks of this study is the observed effects due to residual AnxA2 in KD treatments. We tried to address this problem by using multiple controls. However, better experimental models such as, using gene editing techniques (CRISPR, TALEN) to completely remove AnxA2 or AnxA2 null mouse models are needed to clearly delineate the effects of exo-AnxA2.

In conclusion, our data show that exo-AnxA2 is an important component of the breast cancer – microenvironment signaling. It promotes angiogenesis and vascularization by tPA dependent increase in plasmin generation. Independent of its angiogenesis function we found that exo-AnxA2 also leads to activation of macrophage creating a pre-metastatic aiding in distant organ-specific breast cancer metastasis.

Supplementary Material

Refer to Web version on PubMed Central for supplementary material.

Acknowledgments

Authors would like to thank the UNTHSC Microscopy Core facility, Dr. A. Brun, I. Chang (for technical help), Dr. Sanjay Thamake, and Dr. Mallika Valapala (for valuable experimental input).

Financial support: This work was supported by National Institute on Minority Health and Health Disparities Grant 1P20 MD006882 to JKV.

References

1. Grange C, Tapparo M, Collino F, Vitillo L, Damasco C, Deregibus MC, et al. Microvesicles released from human renal cancer stem cells stimulate angiogenesis and formation of lung premetastatic niche. Cancer research. 2011; 71(15):5346–5356. [PubMed: 21670082]
2. Castellana D, Zobairi F, Martinez MC, Panaro MA, Mitolo V, Freyssinet JM, et al. Membrane microvesicles as actors in the establishment of a favorable prostatic tumoral niche: a role for activated fibroblasts and CX3CL1-CX3CR1 axis. Cancer research. 2009; 69(3):785–793. [PubMed: 19155311]
3. Wysoczynski M, Ratajczak MZ. Lung cancer secreted microvesicles: underappreciated modulators of microenvironment in expanding tumors. International journal of cancerJournal international du cancer. 2009; 125(7):1595–1603. [PubMed: 19462451]
4. Peinado H, Lavotshkin S, Lyden D. The secreted factors responsible for pre-metastatic niche formation: old sayings and new thoughts. Seminars in cancer biology. 2011; 21(2):139–146. [PubMed: 21251983]
5. Yang C, Robbins PD. The roles of tumor-derived exosomes in cancer pathogenesis. Clinical & developmental immunology. 2011; 2011(Journal Article):842849. [PubMed: 22190973]
6. Rescher U, Ludwig C, Konietzko V, Kharitonenkov A, Gerke V. Tyrosine phosphorylation of annexin A2 regulates Rho-mediated actin rearrangement and cell adhesion. Journal of cell science. 2008; 121(Pt 13):2177–2185. [PubMed: 18565825]
7. Lokman NA, Ween MP, Oehler MK, Ricciardelli C. The role of annexin A2 in tumorigenesis and cancer progression. Cancer microenvironment : official journal of the International Cancer Microenvironment Society. 2011; 4(2):199–208. [PubMed: 21909879]
8. Hajjar KA, Acharya SS. Annexin II and regulation of cell surface fibrinolysis. Annals of the New York Academy of Sciences. 2000; 902(Journal Article):265–271. [PubMed: 10865846]
9. Wang J, Betancourt AM, Mobley JA, Lamartiniere CA. Proteomic discovery of genistein action in the rat mammary gland. Journal of proteome research. 2011; 10(4):1621–1631. [PubMed: 21254785]
10. Ling Q, Jacovina AT, Deora A, Febbraio M, Simantov R, Silverstein RL, et al. Annexin II regulates fibrin homeostasis and neoangiogenesis in vivo. The Journal of clinical investigation. 2004; 113(1):38–48. [PubMed: 14702107]
11. Valapala M, Vishwanatha JK. Lipid raft endocytosis and exosomal transport facilitate extracellular trafficking of annexin A2. The Journal of biological chemistry. 2011; 286(35):30911–30925. [PubMed: 21737841]
12. Simpson RJ, Kalra H, Mathivanan S. ExoCarta as a resource for exosomal research. Journal of extracellular vesicles. 2012; 1(Journal Article) 10.3402/jev.v1i0.18374. eCollection 2012.
13. Jeon YR, Kim SY, Lee EJ, Kim YN, Noh DY, Park SY, et al. Identification of annexin II as a novel secretory biomarker for breast cancer. Proteomics. 2013; 13(21):3145–3156. [PubMed: 24019232]
14. Roda O, Valero ML, Peiro S, Andreu D, Real FX, Navarro P. New insights into the tPA-annexin A2 interaction. Is annexin A2 CYS8 the sole requirement for this association? The Journal of biological chemistry. 2003; 278(8):5702–5709. [PubMed: 12468550]
15. Valapala M, Thamake SI, Vishwanatha JK. A competitive hexapeptide inhibitor of annexin A2 prevents hypoxia-induced angiogenic events. Journal of cell science. 2011; 124(Pt 9):1453–1464. [PubMed: 21486955]
16. Lee GY, Kenny PA, Lee EH, Bissell MJ. Three-dimensional culture models of normal and malignant breast epithelial cells. Nature methods. 2007; 4(4):359–365. [PubMed: 17396127]

17. Tavazoie SF, Alarcon C, Oskarsson T, Padua D, Wang Q, Bos PD, et al. Endogenous human microRNAs that suppress breast cancer metastasis. Nature. 2008; 451(7175):147–152. [PubMed: 18185580]
18. Lasser C, Eldh M, Lotvall J. Isolation and characterization of RNA-containing exosomes. Journal of visualized experiments : JoVE. 2012; (59):3037. [PubMed: 22257828]
19. Franzen CA, Simms PE, Van Huis AF, Foreman KE, Kuo PC, Gupta GN. Characterization of uptake and internalization of exosomes by bladder cancer cells. BioMed research international. 2014; 2014(Journal Article) 619829.
20. Sharma S, Rasool HI, Palanisamy V, Mathisen C, Schmidt M, Wong DT, et al. Structural-mechanical characterization of nanoparticle exosomes in human saliva, using correlative AFM, FESEM, and force spectroscopy. ACS nano. 2010; 4(4):1921–1926. [PubMed: 20218655]
21. Merchan JR, Kovacs K, Railsback JW, Kurtoglu M, Jing Y, Pina Y, et al. Antiangiogenic activity of 2-deoxy-D-glucose. PloS one. 2010; 5(10):e13699. [PubMed: 21060881]
22. Drabkin DL, Austin JH. Spectrophotometric studies. II. Preparation from washed blood cells; nitric oxide hemoglobin and sulfhemoglobin. Journal of Biological Chemistry. 1935; 112(Journal Article):51–65.
23. Mineo M, Garfield SH, Taverna S, Flugy A, De Leo G, Alessandro R, et al. Exosomes released by K562 chronic myeloid leukemia cells promote angiogenesis in a Src-dependent fashion. Angiogenesis. 2012; 15(1):33–45. [PubMed: 22203239]
24. Liang Z, Yoon Y, Votaw J, Goodman MM, Williams L, Shim H. Silencing of CXCR4 blocks breast cancer metastasis. Cancer research. 2005; 65(3):967–971. [PubMed: 15705897]
25. Adiseshaiah PP, Patel NL, Ileva LV, Kalen JD, Haines DC, McNeil SE. Longitudinal imaging of cancer cell metastases in two preclinical models: a correlation of noninvasive imaging to histopathology. International journal of molecular imaging. 2014; 2014(Journal Article):102702. [PubMed: 24724022]
26. Jenkins DE, Hornig YS, Oei Y, Dusich J, Purchio T. Bioluminescent human breast cancer cell lines that permit rapid and sensitive in vivo detection of mammary tumors and multiple metastases in immune deficient mice. Breast cancer research : BCR. 2005; 7(4):R444–R454. [PubMed: 15987449]
27. Kadota M, Yang HH, Gomez B, Sato M, Clifford RJ, Meerzaman D, et al. Delineating genetic alterations for tumor progression in the MCF10A series of breast cancer cell lines. PloS one. 2010; 5(2):e9201. [PubMed: 20169162]
28. Kumar R, Yoneda J, Bucana CD, Fidler IJ. Regulation of distinct steps of angiogenesis by different angiogenic molecules. International journal of oncology. 1998; 12(4):749–757. [PubMed: 9499433]
29. Selicharova I, Sanda M, Mladkova J, Ohri SS, Vashishta A, Fusek M, et al. 2-DE analysis of breast cancer cell lines 1833 and 4175 with distinct metastatic organ-specific potentials: comparison with parental cell line MDA-MB-231. Oncology reports. 2008 May; 19(5):1237–1244. [PubMed: 18425382]
30. Barney LE, Dandley EC, Jansen LE, Reich NG, Mercurio AM, Peyton SR. A cell-ECM screening method to predict breast cancer metastasis. Integrative biology : quantitative biosciences from nano to macro. 2015 Feb; 7(2):198–212. [PubMed: 25537447]
31. Png KJ, Yoshida M, Zhang XH, Shu W, Lee H, Rimner A, et al. MicroRNA-335 inhibits tumor reinitiation and is silenced through genetic and epigenetic mechanisms in human breast cancer. Genes & development. 2011 Feb 1; 25(3):226–231. [PubMed: 21289068]
32. Swisher JF, Burton N, Bacot SM, Vogel SN, Feldman GM. Annexin A2 tetramer activates human and murine macrophages through TLR4. Blood. 2010; 115(3):549–558. [PubMed: 19965653]
33. Swisher JF, Khatri U, Feldman GM. Annexin A2 is a soluble mediator of macrophage activation. Journal of leukocyte biology. 2007; 82(5):1174–1184. [PubMed: 17715360]
34. Alderton GK. Metastasis. Exosomes drive premetastatic niche formation. Nature reviewsCancer. 2012; 12(7):447.
35. Peinado H, Aleckovic M, Lavotshkin S, Matei I, Costa-Silva B, Moreno-Bueno G, et al. Melanoma exosomes educate bone marrow progenitor cells toward a pro-metastatic phenotype through MET. Nature medicine. 2012; 18(6):883–891.

36. Wang CY, Lin CF. Annexin A2: its molecular regulation and cellular expression in cancer development. Disease markers. 2014; 2014(Journal Article):308976. [PubMed: 24591759]
37. Alvarez-Erviti L, Seow Y, Schapira AH, Gardiner C, Sargent IL, Wood MJ, et al. Lysosomal dysfunction increases exosome-mediated alpha-synuclein release and transmission. Neurobiology of disease. 2011; 42(3):360–367. [PubMed: 21303699]
38. Zhang Y, Yan W, Collins MA, Bednar F, Rakshit S, Zetter BR, et al. Interleukin-6 is required for pancreatic cancer progression by promoting MAPK signaling activation and oxidative stress resistance. Cancer research. 2013; 73(20):6359–6374. [PubMed: 24097820]
39. Ohishi W, Cologne JB, Fujiwara S, Suzuki G, Hayashi T, Niwa Y, et al. Serum interleukin-6 associated with hepatocellular carcinoma risk: a nested case-control study. International journal of cancerJournal international du cancer. 2014; 134(1):154–163. [PubMed: 23784949]
40. Duda DG, Jain RK. Premetastatic lung “niche”: is vascular endothelial growth factor receptor 1 activation required? Cancer research. 2010; 70(14):5670–5673. [PubMed: 20587530]
41. Psaila B, Kaplan RN, Port ER, Lyden D. Priming the ‘soil’ for breast cancer metastasis: the pre-metastatic niche. Breast disease. 2006; 26(Journal Article):65–74. [PubMed: 17473366]
42. Roshy S, Sloane BF, Moin K. Pericellular cathepsin B and malignant progression. Cancer metastasis reviews. 2003; 22(2–3):271–286. [PubMed: 12785001]

Implications

Exosome associated Annexin A2 plays an important role in angiogenesis and breast cancer metastasis, which can be exploited as a potential biomarker as well as a therapeutic target for diagnosis and treatment of metastatic breast cancer.

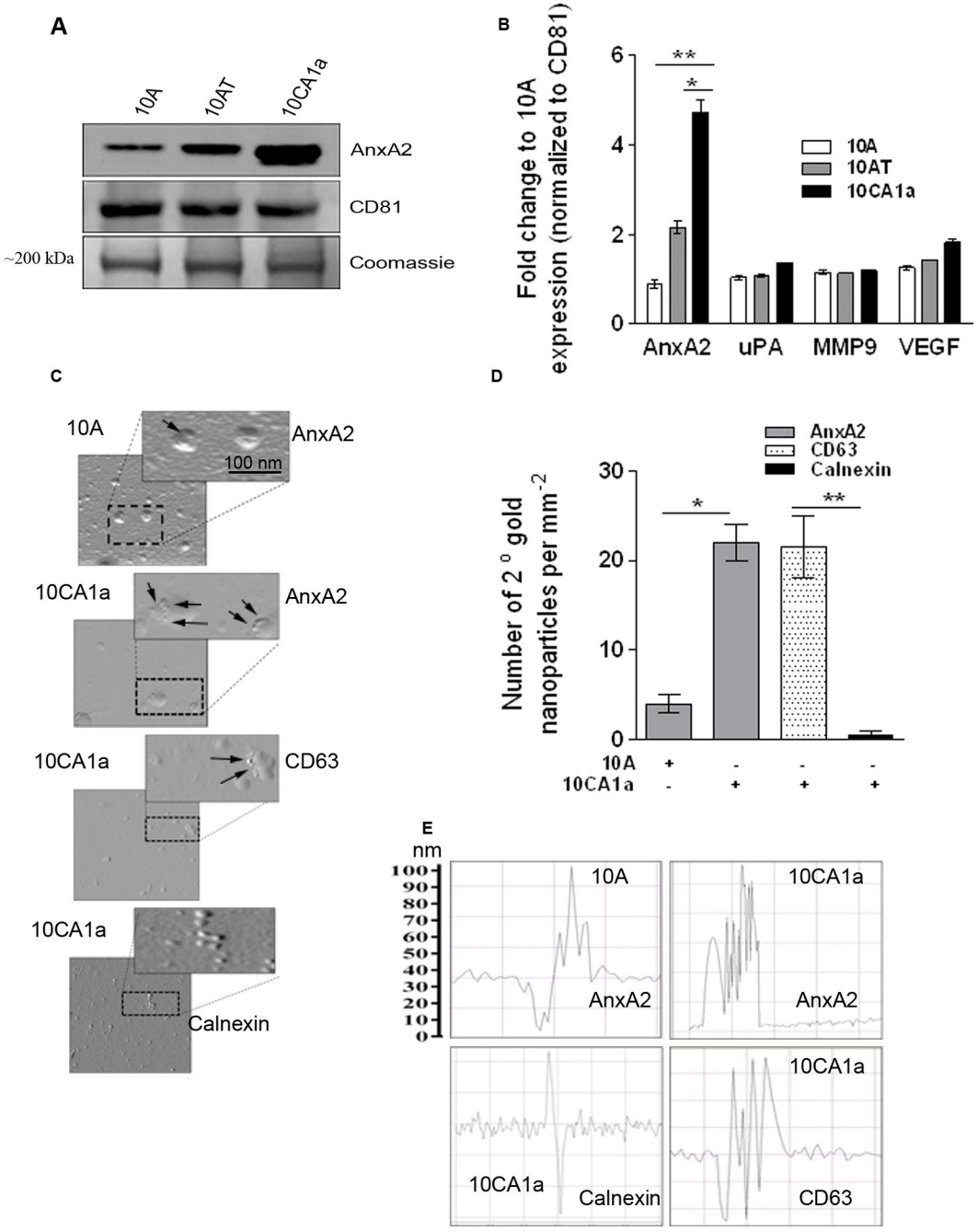

Figure 1. Characterization of exosomes (A–F)

A) Western blot analysis of the different protein levels in the exosomes collected from the MCF10A-, MCF10AT-, and MCF10CA1a-conditioned media. CD81 was used as a loading control (n=3). The Coomassie band confirms equal loading. B) Quantification of the Western blots. Fold change to CD81 is shown. C) Atomic force microscopy (AFM) analysis of MCF10A exosomes and MCF10CA1a exosomes. AnxA2, calnexin, or CD63 immunoreactivity was identified by 25-nm gold nanoparticles. D) Quantification of the AFM data representing the number of secondary gold nanoparticles per field. Four independent

fields were counted. E) Surface topology analysis of the exosomes using the AFM NT-MDT software (n=2). (*) $p < 0.05$, (**) $p < 0.01$, (***) $p < 0.001$, (****) $p < 0.0001$.

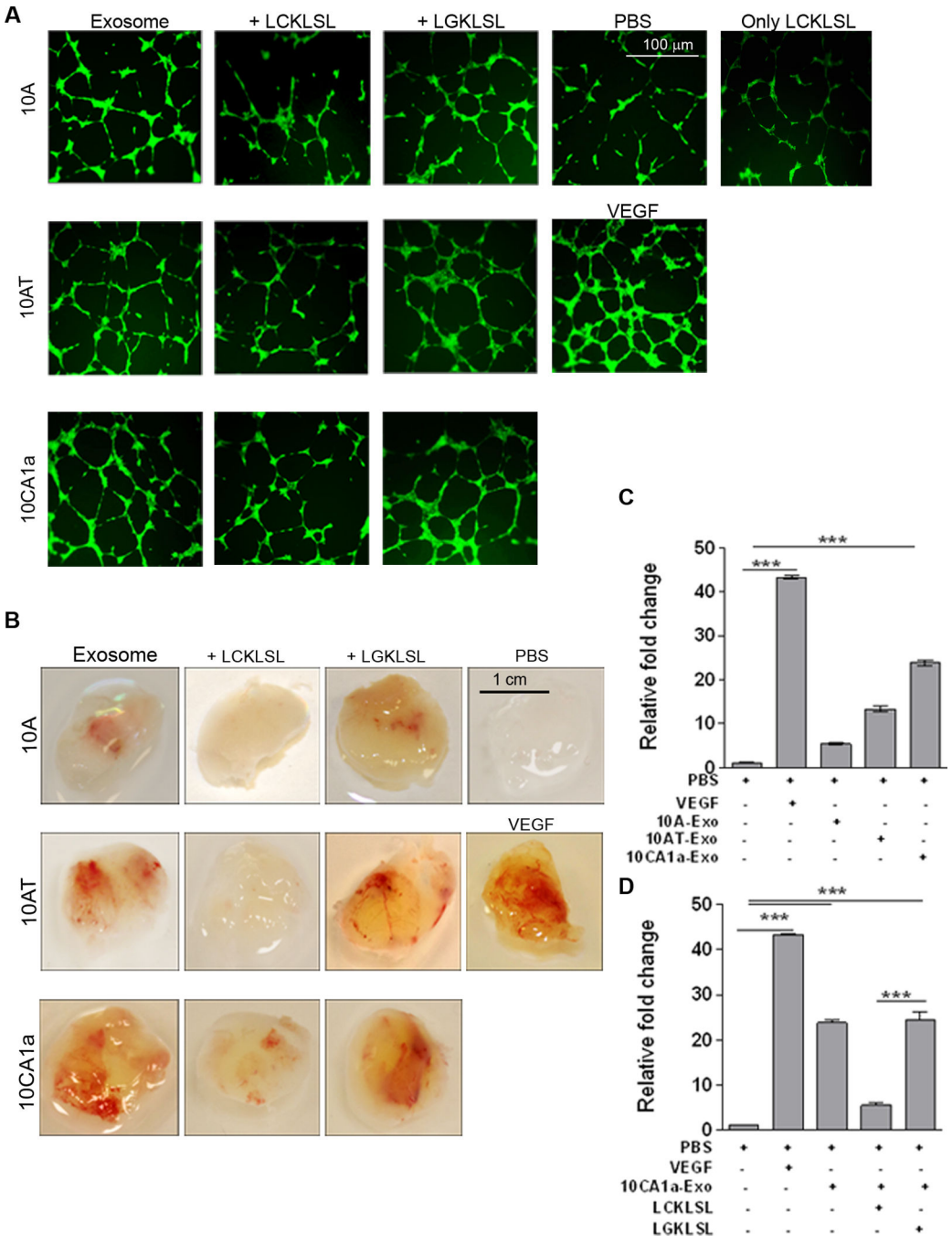

Figure 2. Exo-AnxA2 promotes angiogenesis

Effect of exo-AnxA2 on in vitro tube formation assay. A) Fluorescent images of in vitro endothelial tube formation assay with HUVEC cells; (5 different fields per group were considered. Repeated in triplicates). PBS (negative control), VEGF (100ng/ml, positive control) and 100 µg of exosomal proteins were used (n=3). Peptide concentration used: 5µM (n=3). Exosomes from MCF10A, MCF10AT and MCF10CA1a cells are designated as 10A, 10AT and 10CA1a respectively. Scale bar 100 µm.

Matrigel Plug assay: Mice were injected with matrigel in the presence of PBS alone (negative control), VEGF alone (100 ng/ml, positive control), or 100 μg exosomes ± peptide. After 12 days, the plugs were removed and the angiogenic responses were evaluated. D) Representative images of matrigel plugs are shown. Scale bar 1 cm. Hemoglobin estimation of homogenized matrigel plugs by Drabkin's method (C–D). Fold change to PBS is shown. Peptide concentration: 5μM (n=3). Exosomes from MCF10A, MCF10AT, and MCF10CA1a cells are designated as 10A, 10AT, and 10CA1a, respectively. (*) $p < 0.05$, (**) $p < 0.01$, (***) $p < 0.001$, (****) $p < 0.0001$.

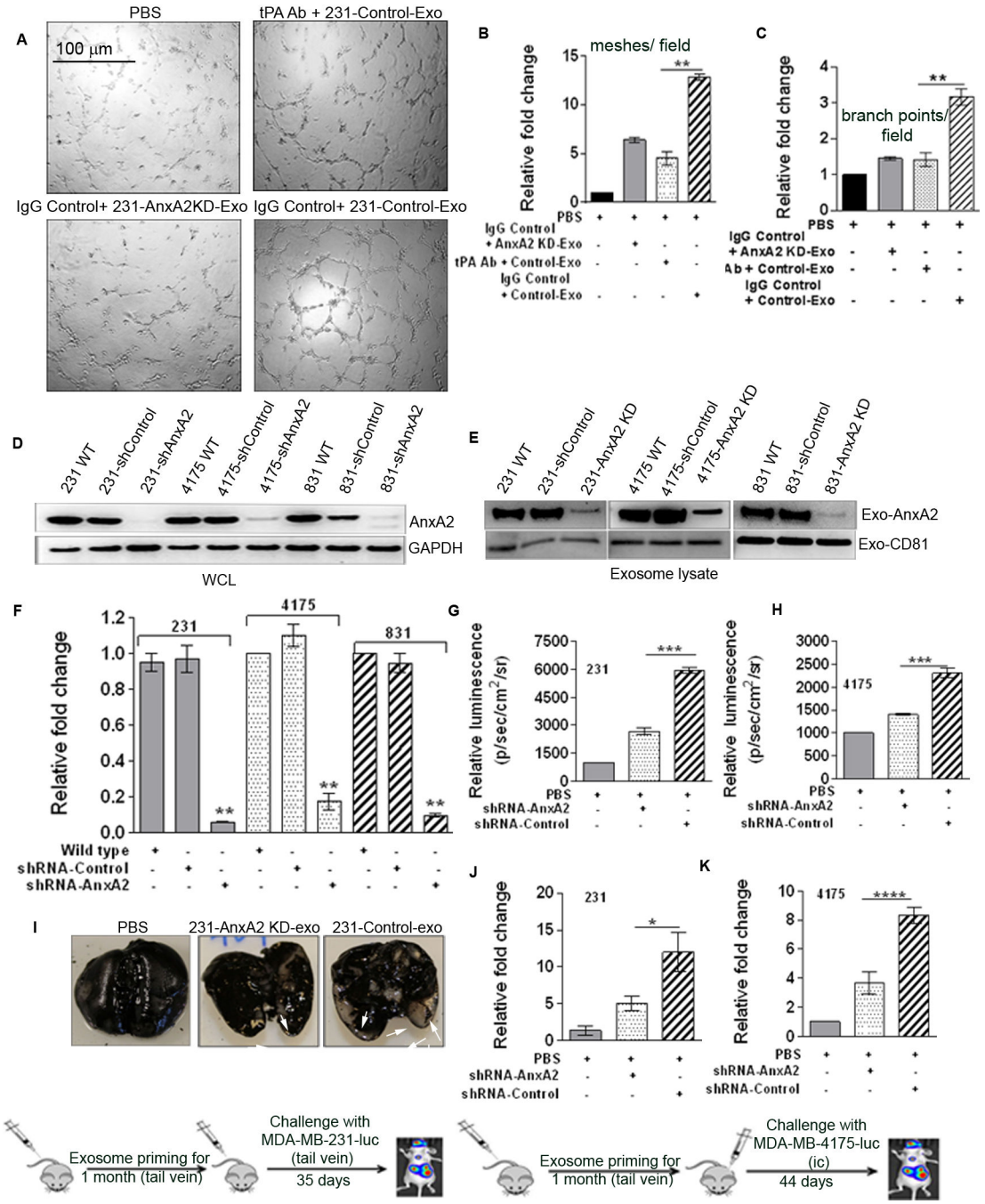

Figure 3. Exo-AnxA2 promotes angiogenesis via tPA and activates macrophages, leading to secretion of IL-6 and TNF-alpha

(A) Endothelial tube formation assay showing the role of tPA in the pro-angiogenic effect of exo-AnxA2 (n=2). Quantification of the number of meshes/field (B) and number of branch points/field (C).

Exo-AnxA2 promotes breast cancer metastasis to lungs . Western blot analysis of WCL (D) and exosomal lysates (E) showing knockdown of AnxA2 (n=2); GAPDH and CD81 were used as loading controls for (D) and (E), respectively. Quantification of exosomal AnxA2 (F). G) Quantification of BLI of PBS-, 231-AnxA2KD-Exo-, or 231-Control-Exo-primed

animals 35 days after challenge with MDA-MB-231-luc cells (lateral tail vein injection), showing differences in the extent of lung metastasis (n=8). Fold change in photon flux to PBS-primed animals is shown. H) Quantification of bioluminescence (BLI) of PBS-, 4175-AnxA2KD-Exo-, or 4175-Control-Exo-primed animals 44 days after challenge with MDA-MB-4175-luc cells (intracardiac; ic) showing differences in the extent of lung metastasis (n=8). Fold change in photon flux to PBS-primed animals is shown. I) India ink staining of the excised lungs from MDA-MB-231-luc cell-injected animals, showing the number of metastatic nodules. Quantification of the number of metastatic lung nodules with MDA-MB-231-luc (tail vein injection) treatment (J) and MDA-MB-4175-luc (ic) treatment (K). Fold change compared to PBS-primed animals is shown. (*) $p < 0.05$, (**) $p< 0.01$, (***) $p < 0.001$, (****) $p < 0.0001$.

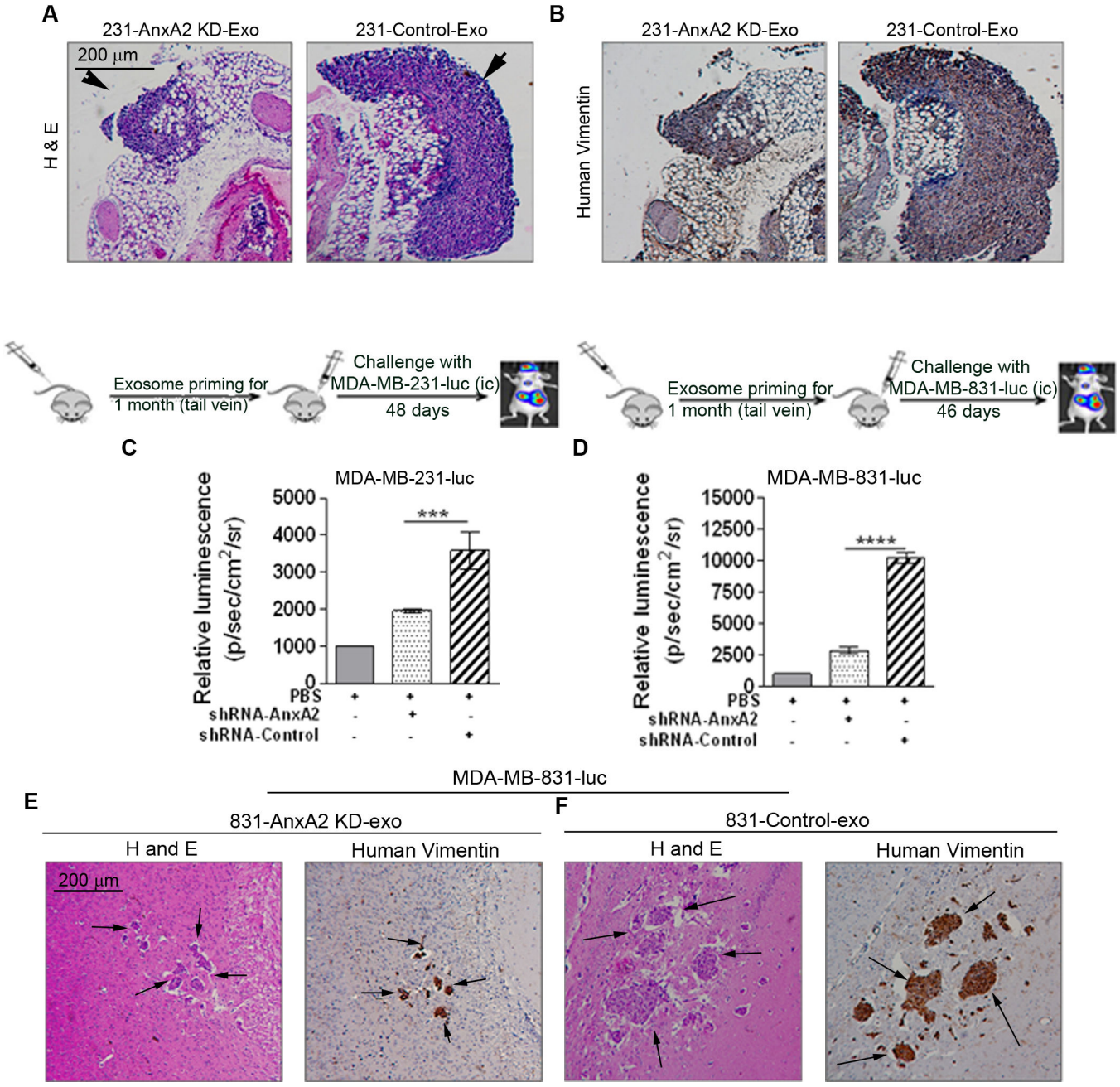

Figure 4.

A) Representative images of H & E staining and DAB immunostaining of the lung sections against human vimentin, showing the localized areas of lung metastasis (n=2). Arrowheads show the metastatic lung nodules. Scale bar 200 μm. All the H & E and DAB images were captured using a Nikon Phase contrast microscope attached to a Canon camera.

Exo-AnxA2 promotes breast cancer metastasis to brain C) BLI quantification in MDA-MB-231-luc-challenged (D) and MDA-MB-831-luc-challenged (E) animals. Fold change in photon flux compared to PBS-primed animals is shown. E-F) Representative images of H & E staining and DAB immunostaining of the brain sections against human vimentin, showing

the localized areas of brain metastasis (n=2). Scale bar 200 μm. All the H & E and DAB images were captured using a Nikon Phase contrast microscope attached to a Canon camera. (*) $p < 0.05$, (**) $p < 0.01$, (***) $p < 0.001$, (****) $p < 0.0001$.

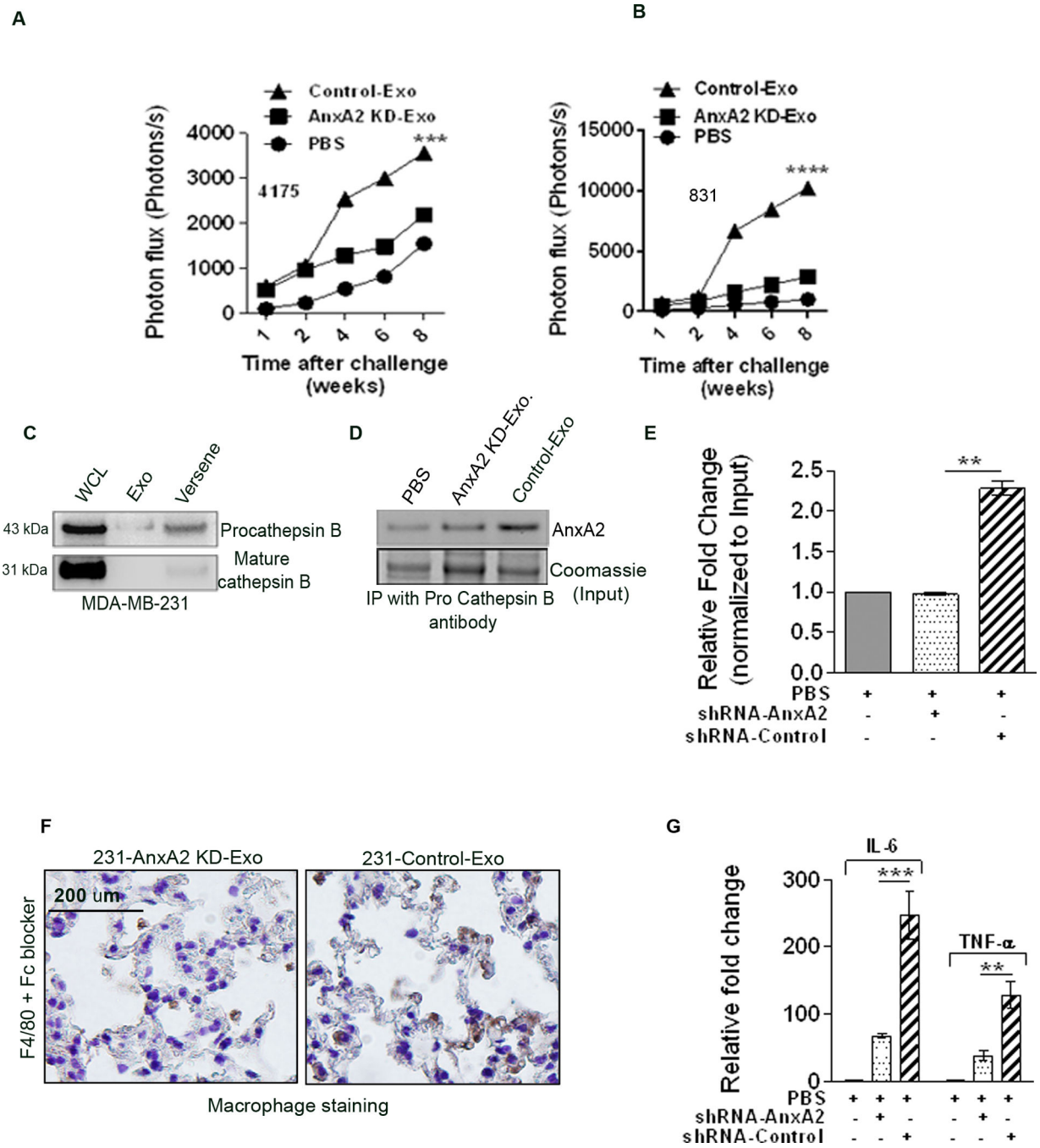

Figure 5.

Quantification of photon flux change over time: (A) MDA-MB-4175-luc-injected lung metastasis and (B) MDA-MB-831-luc-injected brain metastasis. C) Western blot analysis showing the expression of pro-cathepsinB and mature cathepsinB in WCL, Exo lysate, and membrane wash (Versene) fractions. D) Immunoprecipitation of AnxA2 with pro-cathepsinB antibody in the membrane wash lysate after treatment with PBS, AnxA2KD-Exo, or Control-Exo. E) Densitometric analysis of the blot (n=2). (*) $p < 0.05$, (**) $p < 0.01$, (***) $p < 0.001$, (****) $p < 0.0001$. DAB immunostaining of macrophages in the lung

sections with F4/80 antibodies in 231-AnxA2KD-Exo- and 231-Control-Exo-primed animals (F) after Fc blocking. Scale bar = 100 μm. G) ELISA of lung extracts to analyze IL-6 and TNF-alpha levels from PBS-, 231-AnxA2KD-Exo-, and 231-Control-Exo-primed animals, 24 hrs after injection (n=2). (*) $p < 0.05$, (**) $p< 0.01$, (***) $p < 0.001$, (****) $p < 0.0001$.

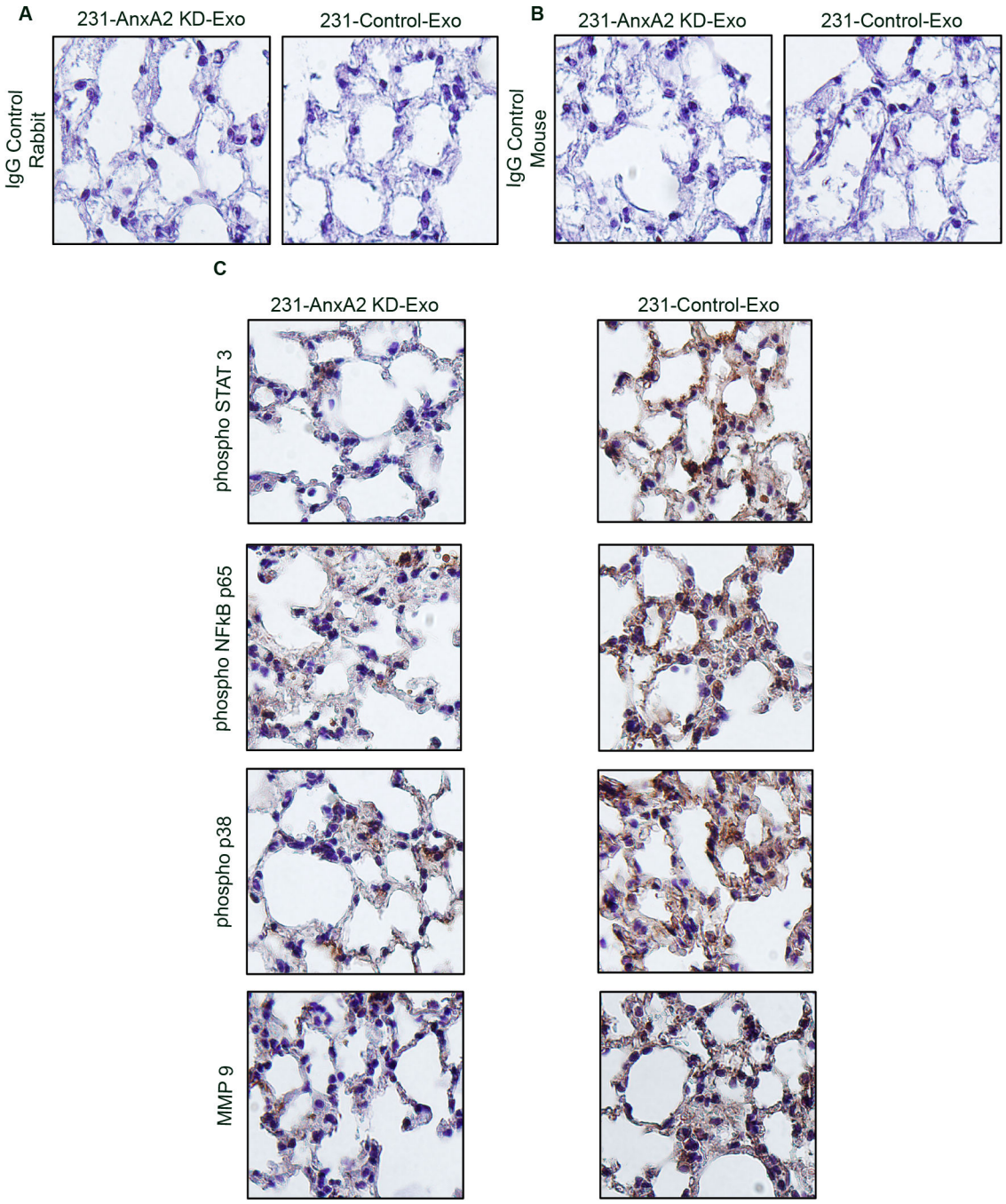

Figure 6. Exo-AnxA2 activates p38-NFκB and STAT3 signaling pathways

Immunohistological analysis of lung sections from 231-AnxA2KD-Exo- and 231-Control-Exo-primed animals. Representative images of DAB immunostaining for the respective proteins are shown. Scale bar 200 μm. (*) $p < 0.05$, (**) $p < 0.01$, (***) $p < 0.001$, (****) $p < 0.0001$.

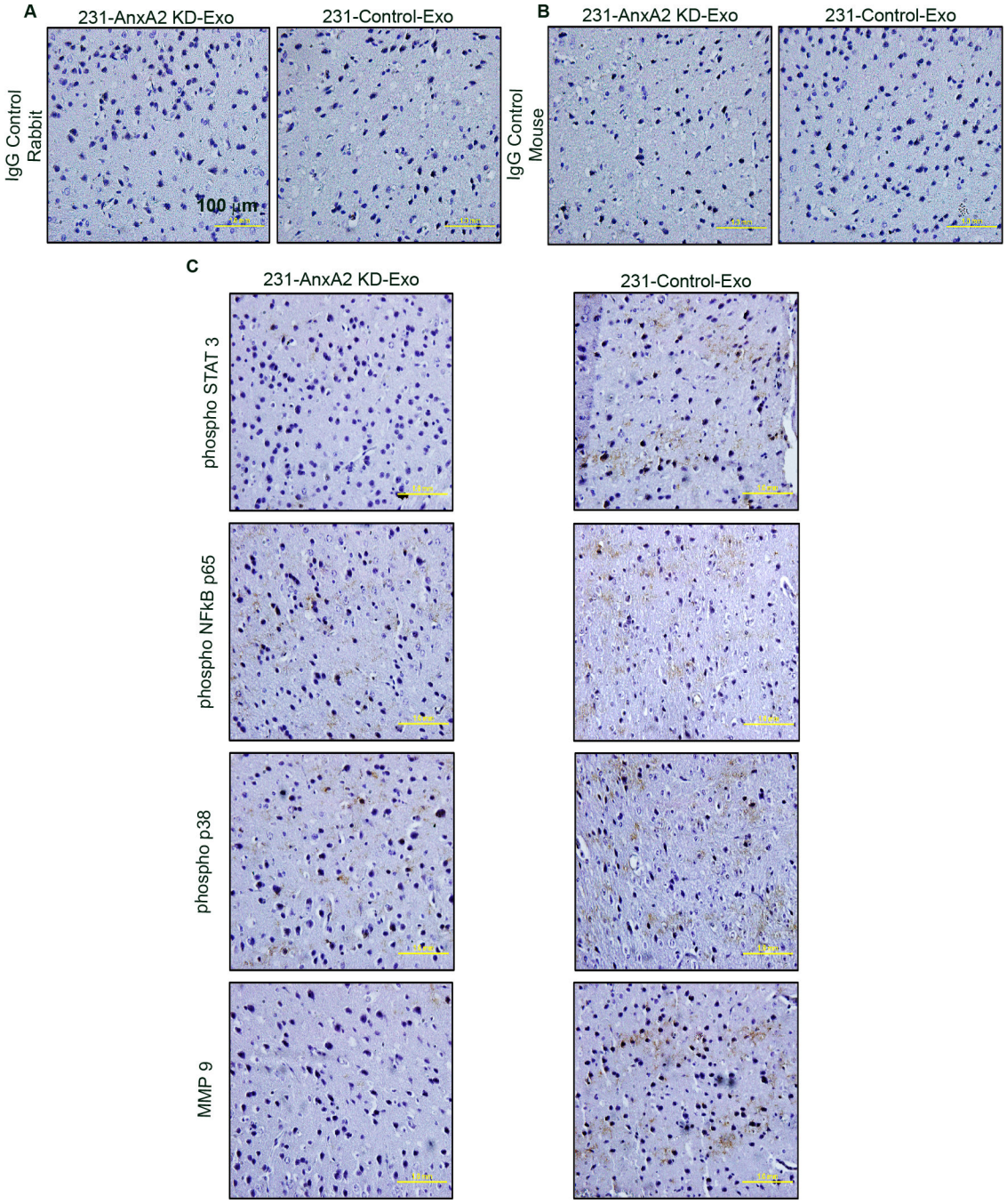

Figure 7. Exo-AnxA2 activates p38-NFκB and STAT3 signaling pathways

Immunohistological analysis of brain sections from 231-AnxA2KD-Exo- and 231-Control-Exo-primed animals. Representative images of DAB immunostaining for the respective proteins are shown. Scale bar 100 μm. (*) $p < 0.05$, (**) $p < 0.01$, (***) $p < 0.001$, (****) $p < 0.0001$.